ELSEVIER

Materials Science and Engineering A231 (1997) 80–89

MATERIALS SCIENCE & ENGINEERING A

The apparent activation energy for the dissolution of spherical Si-particles in AlSi-alloys

F.J. Vermolen, H.M. Slabbekoorn, S. van der Zwaag *

Laboratory of Materials Science, Delft University of Technology, Rotterdamse weg 137, 2628 AL Delft, The Netherlands

Received 7 October 1996; revised 21 February 1997

Abstract

The apparent activation energy for the dissolution of spherical silicon particles in an aluminium matrix is analysed using a numerical dissolution model in which local equilibrium at the particle–matrix interface is assumed. The model takes into account long range diffusion, the temperature dependent solid solubility of silicon in aluminium, the shape of the particle, the finite cell size in which the particle can dissolve and the statistical distribution of the particle size. It is shown that the apparent activation energy can deviate substantially from the activation energy for diffusion, which is the rate controlling process. The model is validated using isoconfigurational annealing experiments at various temperatures for a high purity Al-1.35 mass% Si alloy. An excellent agreement between theory and experiments is obtained. With minor modifications the model can be adjusted to predict the apparent activation energy of (spherical) particle dissolution in other binary systems too. © 1997 Elsevier Science S.A.

Keywords: Activation energy; Dissolution; Si-particles

1. Introduction

Heat treatment of metals is often necessary to optimise their mechanical properties both for further processing and for final use. During the heat treatment the metallurgical state of the material changes. This change can either involve the phases being present or the morphology of the various phases. Whereas the equilibrium phases often can be predicted quite accurately from thermodynamic models, there are no general models for microstructural changes nor general models for the kinetics of these changes. In the latter cases both the initial morphology and the transformation mechanisms have to be specified explicitly. One of these processes, which is both of large industrial and scientific interest and amenable to modelling, is the dissolution of second phase particles in a matrix with a uniform initial composition.

To describe this particle dissolution in solid media several physical models have been developed, incorporating the effects of long-distance diffusion [1–3] and non-equilibrium conditions at the interface [4,5]. The long-distance diffusion models imply that the processes at the interface between particle and matrix proceed infinitely fast. Therefore, these models provide an upper boundary for the dissolution rate.

Whelan [1] considered particles dissolving in an infinite medium using the stationary interface approximation. He derived an analytical solution of the diffusion equation in an infinite medium for spherical co-ordinates by the use of the Laplace-transformation in time. The accuracy of the model increases with increasing interparticle distance, i.e. with increasing cell size.

Baty, Tanzilli and Heckel [2] were the first authors to apply a numerical method using a finite difference method to evaluate the interface position as a function of dissolution time. Their model is also applicable to situations in which the interparticle distance is small, i.e. when soft impingement occurs. Their model was based on the assumption of local equilibrium at all stages of the dissolution process. They applied their numerical analysis to dissolving Al_2Cu-particles in aluminium. The poor fit with the experimental data is probably due to the interface reactions, which were not incorporated into their numerical model.

Tundal and Ryum [3] considered the effects of a finite cell size as well. They too applied a numerical method using a finite difference method to predict the

* Corresponding author.

PII S0921-5093(97)00083-X

dissolution kinetics. Their model was based on the assumption of local equilibrium during the entire dissolution process. They introduced a lognormal distribution for both the particle and cell size and showed that macroscopic dissolution rates depend strongly on the shape of the particle size distribution curve and interactions between the neighbouring cells.

The effect of interfacial reactions on the rate of particle dissolution in both infinite and finite media, i.e. the dissolution of particles under non-local equilibrium conditions, was examined by Vermolen and Van der Zwaag [6]. It was shown that interfacial reactions can have a significant effect on the dissolution rate and hence on the solute concentration profiles in the matrix during particle dissolution.

In all these articles the attention was focused on describing the dissolution kinetics at a single transformation temperature and no attention was paid to the apparent activation energy for particle dissolution as determined from isoconfigurational annealing experiments (i.e. annealing treatments aimed at dissolving a certain fraction of the original particles present). It is this apparent activation energy which is of great technological importance, a.o. for predicting the annealing conditions required for homogenisation of as-cast Al-alloy billets prior to hot extrusion.

The present article describes the apparent activation energy for particle dissolution using a detailed particle dissolution model in which the temperature dependent solid solubility, the shape of the particle, the finite cell size in which the particle can dissolve and the statistical distribution of the particle size are taken into account. As in other models [1–3] local equilibrium at the particle–matrix interface is assumed at all times, i.e. rate limiting interfacial reactions are excluded. The model is of a general nature but the effects of the various parameters in the model on the dissolution kinetics are shown explicitly for the Al–Si system. From the work by Tundal and Ryum [3] and our own preliminary experiments [7] it can be concluded that in the Al–Si system Si particle dissolution proceeds under local equilibrium conditions. Furthermore, thermomechanical treatments can be designed to generate a microstructure of approximately spherical Si particles in an aluminium matrix with a uniform Si concentration, making the Al-1.35 mass% Si system an excellent system to validate the model predictions.

2. Theory

The model used to determine the kinetics of particle dissolution is based on several physical assumptions. For completeness the physical assumptions and the originating initial boundary value problem are sketched first. Subsequently, the influence of each assumption in the model on the apparent activation energy for particle dissolution is shown.

2.1. The model

The model treats a binary system with limited solubility of B-atoms in the α-phase (see Fig. 1(a)) and no solubility of A-atoms in the β-phase (i.e $c^{\beta/\alpha} = 100\%$). For compositions corresponding to the two phase region at the starting temperature T_{ini}, the material with an average composition c^0 is assumed to consist of equally sized spherical β-phase particles of radius R_0, in a uniform matrix consisting of an α phase of composition c^m. Upon raising the temperature to the homogenisation temperature T_{dis} the solubility of B in α increases, provided T_{dis} is lower than the eutectic temperature T_{eut}, and the particle starts to dissolve. The solubility at the homogenisation temperature is denoted as $c^{\alpha/\beta}$. Each β particle is assumed to dissolve in a surrounding spherical cell of radius R_c. The average interparticle distance L can be used to calculate the radius of the equivalent spherical cell in which the particle dissolves:

$$R_c = L\sqrt[3]{\frac{3}{4\pi}} \qquad (1)$$

Assuming the total number of B-atoms in each cell to be constant, net transfer of B-atoms between the cells is excluded. This implies:

$$\partial c(R_c, t)/\partial r = 0 \qquad (2)$$

The assumption of local equilibrium at the α/β interface yields boundary condition

$$c(R(T), t) = c^{\alpha/\beta} \qquad (3)$$

During dissolution B-atoms migrate away from the interface. No diffusion inside the particle is assumed.

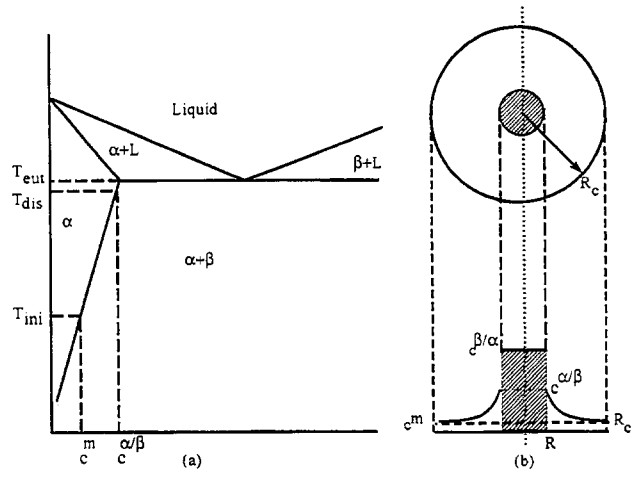

Fig. 1. A schematic binary phase diagram (a) and a spherical particle in a spherical cell (b).

Application of Fick's second law for a planar ($m=0$), cylindrical ($m=1$) and spherical ($m=2$) symmetry yields:

$$\frac{\partial c(r,t)}{\partial t} = D\left[\frac{\partial^2 c(r,t)}{\partial r^2} + \frac{m}{r}\frac{\partial c(r,t)}{\partial r}\right] \quad \begin{matrix} \forall R(t) < r < R_c \\ \forall \geq 0 \end{matrix} \tag{4}$$

The diffusion coefficient, D (in $m^2\ s^{-1}$), is taken to be independent of composition.

The initial boundary value problem, defined by Eqs. (2)–(4) has a solution, if and only if $c(r,t)$ has continuous derivatives at least up to the second derivative with respect to r, at the interval $R<r<R_c$ and up to the first derivative with respect to t for all $t>0$. Moreover, it can be proven that the solution of Eq. (4) is unique [8]. As the number of B-atoms in the cell is constant, it can be derived that:

$$\frac{dR(t)}{dt} = \frac{D}{\left(\frac{\rho_\beta}{M_\beta}c^{\beta/\alpha} - \frac{\rho_\alpha}{M_\alpha}c(R(t),t)\right)}\frac{\rho_\alpha}{M_\alpha}\left(\frac{\partial c(r,t)}{\partial r}\right)_{r\downarrow R(t)}, \quad \forall \geq 0 \tag{5}$$

Here ρ_α and ρ_β are the densities of the pure phases α and β density changes as a function of composition have been neglected), M_α and M_β are the molar masses of the pure phases α and β.

From Eq. (5) it follows that the value of $\partial c(R,t)/\partial r$ determines the value of $dR(t)/dt$. Apparently, the amount of B-atoms present in the immediate vicinity of the dissolving particle governs the rate of the interface velocity $dR(t)/dt$. The initial boundary value problem thus defined falls into the class of Stefan problems with a free boundary [9,10].

Summarising, the parameters in the model which affect the dissolution kinetics are the diffusion coefficient D, the temperature dependent solubility, $c^{\alpha/\beta}$, the geometry of the system as defined by the shape of the particle and the ratio of the particle to cell size. Furthermore, as small particles are known to dissolve faster than large particles, the initial particle size distribution will have an effect on the apparent dissolution kinetics too. The effects of these parameters are considered in succession, using numerical values for the Al–Si system where appropriate.

2.2. The activation energy for diffusion

The diffusion coefficient of silicon in aluminium is given by an Arrhenius relation which has been experimentally determined by Fujikawa [11], and which is given by:

$$D = D_0 \exp\left(-\frac{Q_{\text{diffusion}}}{RT}\right) \tag{6}$$

For the system considered the activation energy for diffusion of silicon in aluminium, $Q_{\text{diffusion}}$, is 136 kJ mol^{-1} and D_0. equals 2.02 $cm^2\ s^{-1}$. This contribution to the activation energy of particle dissolution is referred to as the diffusional activation energy. The other components of the activation energy are determined by the refinement of the dissolution models by the step by step incorporation of the different relevant aspects into the dissolution model.

2.3. The activation energy due to the temperature dependent solid solubility

The solid solubility of silicon in aluminium can be obtained as a function of temperature from the binary AlSi-phase diagram reported in literature [12]. To determine its effect on the dissolution kinetics, all contributions caused by geometry, finiteness and particle size distributions have to be excluded. Therefore, the dissolution of an infinite plate of finite thickness in an infinite medium has been considered first. For this case it can be derived that [5]:

$$t_\gamma = \frac{\pi(1-\gamma)^2\xi_0^2}{4k^2D} \quad \text{with } k = \frac{c^{\alpha/\beta}-c^m}{c^{\beta/\alpha}-c^{\alpha/\beta}}, \quad \xi(0)=\xi_0$$
$$\text{and} \quad \gamma = \frac{\xi(t)}{\xi_0} \tag{7}$$

In which t_γ is the time needed to dissolve the β-phase into the α-phase such that the ratio between the final and initial β-phase volume fraction equals γ, ξ_0 and $\xi(t)$ respectively are the initial and residual plate thickness in m. $c^{\alpha/\beta}$ is the solid solubility of silicon in aluminium in mass fraction, $c^{\beta/\alpha}$ is the mass fraction of silicon in the particle, which equals unity and c^m is the initial mass fraction of silicon in the aluminium rich matrix (Fig. 1(b)).

Taking the logarithm of Eq. (7) yields:

$$\ln(t_\gamma) = 2\ln\left(\frac{(1-\gamma)\sqrt{\pi}\xi_0}{2k}\right) - \ln(D) \tag{8}$$

In Eq. (8) only the factors k and D depend on temperature, therefore Eq. (8) can be read as:

$$\ln(t_\gamma) = C - 2\ln(k) - \frac{Q_{\text{diffusion}}}{RT} \tag{9}$$

Here C is a constant which is determined by the ratio of the final and initial plate thickness. The effect of the solid solubility $c^{\alpha/\beta}$ is incorporated in the parameter k. Fitting the discrete values of the solid solubility, provided by Mondolfo [12] to a fourth order polynomial with respect to the dimensionless reciprocal temperature, T_{eut}/T one obtains:

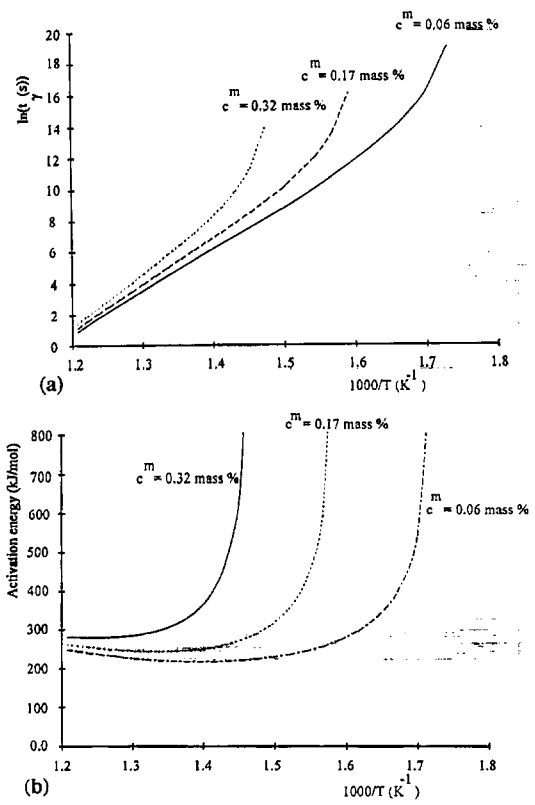

Fig. 2. The logarithm of the dissolution time (a) and the apparent activation energy (b) as a function of the reciprocal temperature for a flat plate dissolving in an infinite medium for three different values of the initial Si concentration in the matrix with $\gamma = 0.99$.

$$-\ln(k)\left(\frac{1}{T}\right) = -76.49 + 185.99\left(\frac{T_{eut}}{T}\right) - 129.43\left(\frac{T_{eut}}{T}\right)^2 + 13.76\left(\frac{T_{eut}}{T}\right)^3 + 10.30\left(\frac{T_{eut}}{T}\right)^4 \quad (10)$$

Where T is the absolute temperature in Kelvin and T_{eut} is the eutectic temperature in Kelvin. The above equation is valid over the temperature range 573 K < T < 850 K. Eqs. (9) and (10) show a clear dependence of the activation energy of particle dissolution on the boundary conditions that are imposed by thermodynamics. From Eq. (9) it also follows that for the case of a flat infinite plate the activation energy for dissolution does not depend on the fraction dissolved.

Fig. 2(a) displays the time required to reduce the plate thickness to 99% of its initial thickness as a function of the reciprocal temperature for three initial matrix compositions. The asymptotic behaviour of the dissolution time for high reciprocal temperatures is due to the decrease of the solid solubility with decreasing temperature such that the solid solubility, $c^{\alpha/\beta}$, approaches to the initial mass fraction of Silicon in the Aluminium rich phase, c^m. From Eqs. (7) and (9) it can be seen that there is a singularity at $c^{\alpha/\beta} = c^m$. Fig. 2(b) displays the apparent activation energy for the same initial conditions as used for calculating the curves in Fig. 2(a). The figure shows that the activation energy is more or less constant for temperatures well in excess of the temperature at which $c^{\alpha/\beta} = c^m$. Even in this temperature range the apparent activation energy (200–260 kJ mol^{-1}) is considerably larger than that for diffusion of Si in Al (136 kJ mol^{-1}) due to the temperature dependence of the solid solubility. It can be shown that the weak minimum in Fig. 2(b) is related to the polynomial fit used to describe the solid solubility.

2.4. The activation energy due to the spherical geometry of the particle

The next refinement of the dissolution model consists of the consideration of the geometrical contribution to the activation energy. To illustrate this effect, spherical particles have been considered. The dissolution time of a spherical particle in an infinitely large medium can be determined by [1]:

$$\ln\left(\frac{R^2(t) + 2bR(t)\sqrt{t} + 2at}{R_0^2}\right) = -\frac{2b}{\sqrt{2a-b^2}}\arctan\left(\frac{\sqrt{2a-b^2}}{\frac{R(t)}{\sqrt{t}} + b}\right) \quad \text{with } a = kD \text{ and } b = k\frac{D}{\sqrt{\pi}} \quad (11)$$

With the above equation, particle dissolution times have been calculated as a function of the dissolution temperature. Fig. 3(a) displays the logarithm of the dissolution time as a function of the reciprocal temperature for different residual particle volume fractions. The initial matrix concentration, c^m, was 0.06 mass% for all curves. The apparent activation energy for the cases considered in Fig. 3(a) has been plotted in Fig. 3(b). As dissolution proceeds the particle area decreases. As a result of this, to dissolve a fixed volume of the particle, the radial translation of the particle surface required must increase. This explains the decrease of the activation energy for the dissolution of a spherical particle with proceeding dissolution as can be seen in Fig. 3(b) for different residual fractions of the original particle volume. The differential geometrical contribution to the apparent activation energy (Q_{dif}) can be defined as the energy needed to increase the dissolved fraction of a spherical particle from $1-\gamma$ to $1-\gamma-d\gamma$. γ is the ratio of the residual and the initial volume fraction of the particle. In other words, the differential geometrical contribution to the activation energy is related to the geometrical contribution to the apparent activation energy as follows:

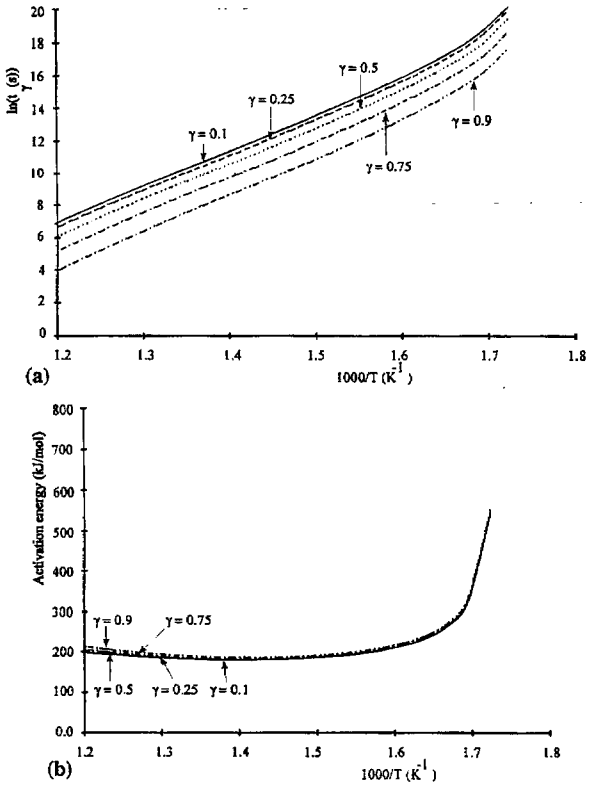

Fig. 3. The logarithm of the dissolution time (a) and the apparent activation energy (b) as a function of the reciprocal temperature for a sphere dissolving in an infinite medium for an initial matrix concentration of 0.06 mass%. $\xi_{final}/\xi_0 = 0.01$ for various values of γ.

$$Q_{\text{geometric}} = \int_1^{1-\gamma} Q_{\text{dif}}(\tilde{\gamma})\, d\tilde{\gamma} \qquad (12)$$

Differentiation of the activation energy with respect to the fraction dissolved yields the differential activation energy. The differential geometrical contribution to the apparent activation energy has been plotted as a function of volume fraction dissolved in Fig. 4, for the same set of input parameters as in Fig. 3.

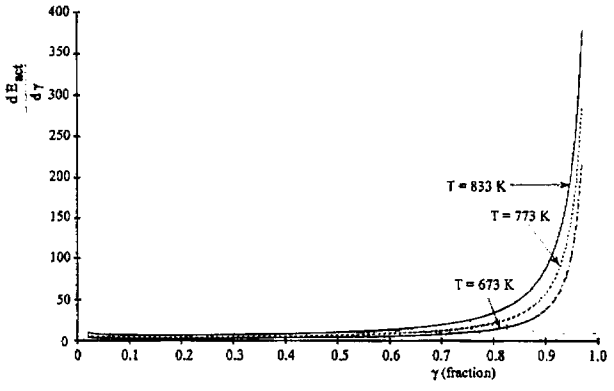

Fig. 4. The differential geometrical contribution to the apparent activation energy as a function of the fraction dissolved for three different temperatures and an initial matrix concentration of 0.06 mass%.

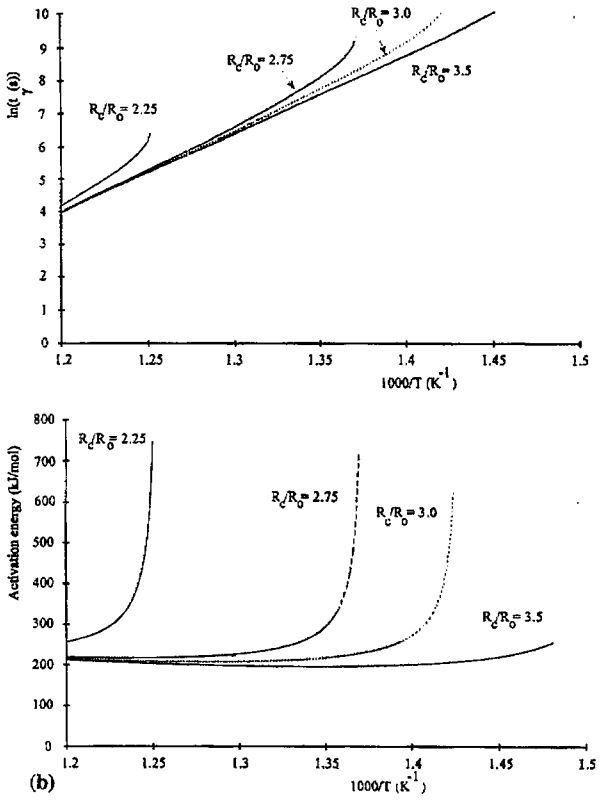

Fig. 5. The logarithm of the dissolution time (a) and the apparent activation energy (b) as a function of the reciprocal temperature for a sphere dissolving, until a residual volume fraction of 0.90 has been reached, for four R_c/R_0-ratios. The initial matrix concentration was 0.06 mass%.

2.5. The activation energy due to the finite cell size

The alloy has been assumed to consists of a set of discrete cells in each of which only one particle dissolves. To investigate the influence of the interaction between diffusion fields, i.e. soft-impingement effects, a finite difference discretisation technique has been used to solve the diffusion equation with a moving boundary and finite cell size [13]. The logarithm of the dissolution time for a sphere until $\gamma = 0.90$ has been plotted as a function of the reciprocal temperature in Fig. 5(a) for different cell sizes taking into account the temperature dependent solid solubility. The initial matrix concentration, c^m, was 0.06 mass% and the initial particle radius, R_0, was 5 μm for all curves. In Fig. 5(b) the activation energy for the dissolution of a sphere until $\gamma = 0.90$ with respect to the reciprocal temperature has been plotted using the same cell sizes as in Fig. 5(a). The difference between the curves in Fig. 5(b)Fig. 3(b) can be regarded as the contribution of the effects of soft-impingement to the activation energy $Q_{\text{soft-impingement}}$.

2.6. The activation energy due to the statistical distribution of the cell size

As shown in the previous paragraph the dissolution kinetics depends on the size of the particle and the cell in which it dissolves. Since in practice materials will contain particles with a distinct size distribution, the width of the distribution will affect the temperature dependent dissolution kinetics and hence the apparent activation energy. A commonly observed particle size distribution is the log-normal distribution function given by:

$$F(R) = \frac{1}{\sqrt{2\pi}\,\ln(\sigma_{geo})R}\exp\left(\frac{(\ln(R)-\ln(\mu_{geo})^2}{2(\ln(\sigma_{geo}))^2}\right) \quad (13)$$

In which μ_{geo} and σ_{geo} respectively are the geometrical mean and the geometrical standard deviation of the particle size. In the calculations this distribution function has been replaced by an equivalent set of 100 particle size classes. In each class the cell size was taken such that the average composition in each cell was equal to the nominal composition.

In Fig. 6(a) the effect of the width of the geometrical standard deviation of the particle size distribution, taking the average particle size constant, is shown. The residual volume fraction, α, was 0.95 for all curves. All particles dissolve in cells such that the initial matrix concentration and the average concentration of B-atoms are equal to 0.26 and 1.35 mass% respectively. As the concentration of B-atoms equals 100 mass% in the particle, there is a unique correspondence between the cell size and the particle size.

The figure shows that the time required to dissolve 5% of the total particle volume clearly depends on the width of the particle size distribution. As expected, the effect of the width of the distribution on the apparent activation energy is negligible at sufficiently high temperatures and only becomes significant for temperatures where the average concentration equals the solid solubility.

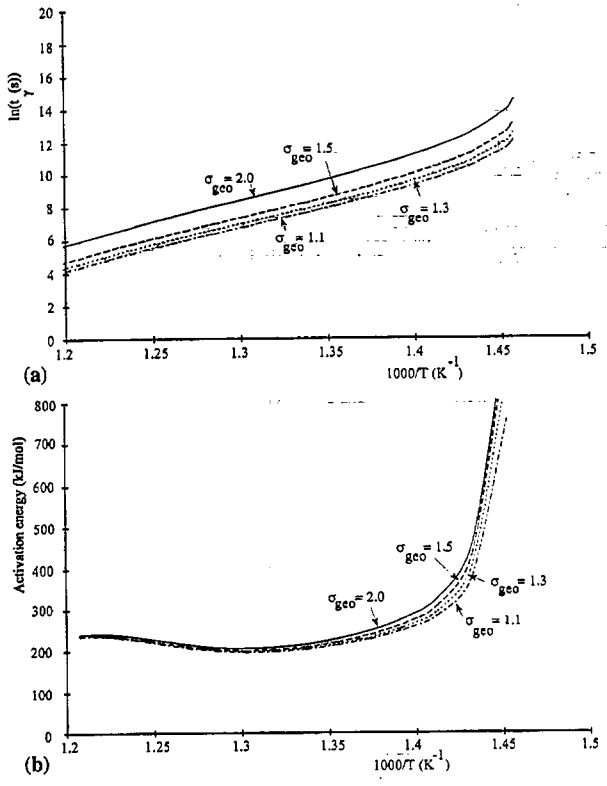

Fig. 6. The logarithm of the dissolution time until a residual volume fraction of 0.95 has been reached (a) and the apparent activation energy (b), for an alloy with an initial silicon concentration in the matrix of 0.26 mass% and a total silicon concentration of 1.35 mass%, as a function of the reciprocal temperature for different standard deviations of the particle size distribution.

3. Validation of the model

The model is validated using a high purity Al-1.35 mass% Si alloy. The Al–Si system was selected on the basis of the earlier work by Tundal and Ryum [3] from which could be concluded that interfacial phenomena have no effect on the dissolution kinetics, i.e. local equilibrium prevails at all stages of the dissolution process. This was confirmed by our preliminary isothermal dissolution experiments and measurement of the Si concentration profile in the vicinity of Si particles after partial dissolution [7].

To obtain a microstructure which resembles the microstructure assumed in the model, i.e. spherical Si particles in an Al matrix with a uniform Si concentration, a thermomechanical pre-treatment on the as cast material has been carried out prior to the dissolution experiments. The experimental conditions during the pre-treatment and subsequent dissolution experiments are described below.

3.1. Pre-treatment

The Al-1.35 mass% Si alloy was obtained by melting the appropriate mixture of 99.99% pure aluminium and 99.999% silicon and metal mould casting. Spectroscopic analysis of the as-cast material revealed an average Si concentration of 1.35 mass% and a Fe concentration of less than 0.005 mass%. No other trace elements were found at concentration levels in excess of 0.005%.

After casting, the as-cast material was annealed during 120 h at 840 K. To avoid surface oxidation the alloy was contained in a stainless steel bag flushed with de-oxidised nitrogen gas during this annealing treatment. Optical observation of the annealed material, using a Keller and Wilcox solution as etchant, revealed that almost all Si particles had dissolved, leaving a homogeneous dendritic microstructure. To break up the

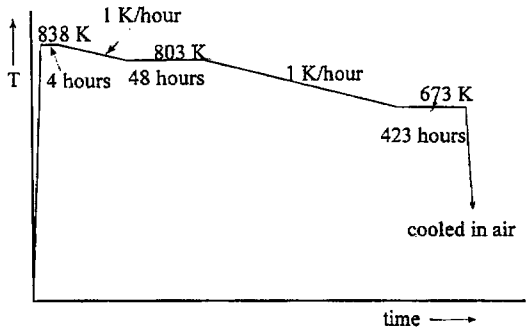

Fig. 7. The temperature-time diagram for the thermal pre-treatment of the experimental alloy.

dendritic microstructure and to generate large spherical grains, a 6-pass cold rolling and intermediate recrystallisation treatment was applied. The recrystallisation temperature was 623 K with an annealing time of 1 h.

Following these deformation and recrystallisation treatments the sample received a final heat treatment to generate large spherical Si particles in an Al matrix of uniform composition. This final treatment is shown in Fig. 7. First, the sample was annealed for 4 h at 838 K to dissolve any particles formed during the interpass recrystallisation treatment. Subsequently, the sample was cooled at a rate of 1 K h^{-1} to a temperature of 803 K. This temperature is just below the temperature at which 1.35 mass% Si will stay in solid solution. The sample was annealed at this temperature for another 48 h. The slow cooling and the intermediate annealing aimed at generating a low nucleation site density for Si particle formation. Then, the sample was cooled to 673 K at a rate of 1 K h^{-1}. This cooling rate and the subsequent final annealing for 423 h at this temperature was selected on the basis of a separate computer model, to obtain a condition of a low but uniform Si concentration in the matrix surrounding each Si particle in as short a time as possible. After annealing at 673 K the sample was air cooled to room temperature and the sample was cut into smaller pieces.

The Si concentration profile around the Si particles in the pre-treated material was measured using electron microprobe analysis (EPMA). A typical result of such a measurement is shown in Fig. 8. As shown in the figure a uniform Si concentration of 0.26 mass% has been obtained in the Al matrix. The apparent increase in Si concentration in a small region near the interface is an artefact due to the lateral dimension of the electron beam (typically 2 mm). It should be pointed out that this Si concentration in solid solution is considerably higher than Si solubility at room temperature, which is negligible. The Si concentration in solution is clearly kinetically determined.

The Si particle size distribution and the total area fraction of Si particles was determined using quantitative optical microscopy techniques and a computerised image analysis system (Leitz CBA 8000) on etched samples. The recorded 2-D particle size distribution was converted into the true 3-D particle size distribution using the method outlined in [14]. The particle size distribution in Table 1 resulted.

The particle size distribution resembles a log-normal distribution (geometrical mean $\mu = 4.515$ μm and geometrical standard deviation $\sigma = 1.64$ μm).

The initial volume fraction Si particles determined metallographically is $f_{init} = (1.37 \pm 0.21)$ vol.%, which is in agreement with the volume fraction calculated on the basis of the overall composition and the Si concentration in solid solution determined by EPMA.

3.2. The iso-configurational experiments

Using the initial particle size distribution and the initial Si concentration in the matrix as input parameters in the model, the isothermal dissolution kinetics could be calculated. From these calculations the times required at each temperature to reach a certain fraction of the total initial volume of Si particle (i.e. an iso-configurational state) could be determined. A residual fraction, γ of 64% was selected as the target residual fraction for the dissolution experiments. At this residual volume fraction the experiments can be performed over a wide temperature range within reasonable annealing times, while the reduction in total particle volume can be determined with sufficient experimental accuracy.

The appropriate isothermal annealing conditions derived from the calculations which were used in the experiments are listed in Table 2. Heating and cooling times were of the order of 1 min and 10 s respectively and can be ignored with respect to the annealing times.

Following the dissolution treatment the remaining particle size distribution and the remaining particle volume fraction were determined using the metallographic techniques just described. A surface layer of approximately 1 mm was removed mechanically prior to specimen preparation to get rid of any surface reaction effects during homogenisation. The remaining

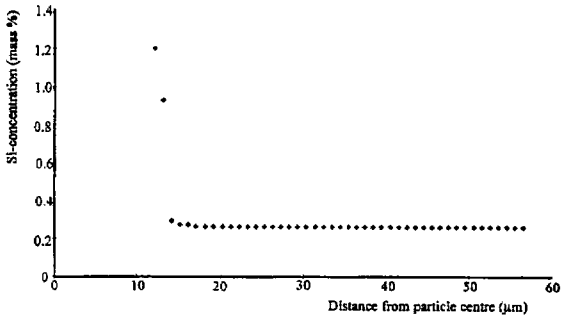

Fig. 8. The Si concentration profile in the matrix surrounding a spherical particle as determined by EPMA for the pre-treated sample.

Table 1
The actual particle size distribution present in the alloy

Size (μm)	2	6	10	14	18	22	26	30	34	38
No. per mm^3	1230	5720	1280	422	122	232	398	199	4	29

volume fraction silicon particles, f_{final}, experimentally determined is also listed in Table 2.

4. Results

The results of the metallographic measurement of the remaining total Si particle volumes at the four annealing temperatures are listed in Table 2 and are shown in Fig. 9. An excellent agreement between the measured and the intended residual volume fraction $\gamma = 0.64$ is observed. The experimental data lead to an apparent activation energy for particle dissolution of (280 ± 5) kJ mol^{-1}.

5. Discussion

The excellent agreement between experimental results and theoretical predictions is in strong support of the model presented, in particular as there are no (arbitrarily) adjustable parameters in the model. As the time required to dissolve a certain fraction of the Si particles clearly depends on several other factors apart from the dissolution temperature, it is instructive to examine the influence of each of these factors on the annealing time required using the range of annealing temperatures and the alloy composition employed in the experiment. This is shown in Fig. 10 which shows the dissolution times required to reach $\gamma = 0.64$ for various situations to be just described. In the figure the conditions leading to $\gamma_{experimentally} = 0.64$ are indicated too. In all subsequent calculations the Si concentration in the matrix was kept at 0.26 mass%. Curve I in Fig. 10 applies to the case of a single planar particle of finite thickness but of infinite width dissolving in an infinite medium assuming the solid solubility of Si in the matrix to be constant at $c^{\alpha/\beta} = 0.655$ mass%. This model clearly overestimates the experimentally verified times required to reach the condition $\gamma = 0.64$. Of course the degree of overestimation depends strongly on the value of the solid solubility chosen. As in this case the diffusion is the only temperature dependent factor, the apparent activation energy for particle dissolution is constant and equal to that for volume diffusion of Si in Al (136 kJ mo^{-1}). Curve II applies to the situation of curve I but taking the solid solubility of Si in Al to be temperature dependent (Eq. (10)). Due to the temperature dependence of the solid solubility the slope of curve II is steeper than that of curve I and the activation energy is no longer constant. However, the dissolution times required are still overestimated considerably. Curve III applies to the situation of curve II but taking the particle to be spherical rather than planar. Due to the higher interfacial area to particle volume ratio the dissolution is significantly accelerated. For these conditions the disso-

Table 2
Isothermal annealing conditions and the residual volume fraction Si particles determined experimentally

Temperature (K)	Time (s)	f_{final} (vol.%)	γ (—)
783	1.2×10^5	0.93 ± 0.26	0.68 ± 0.16
823	1.4×10^3	0.92 ± 0.25	0.67 ± 0.17
833	9.0×10^2	0.88 ± 0.21	0.64 ± 0.12
843	5.8×10^2	0.88 ± 0.25	0.65 ± 0.16

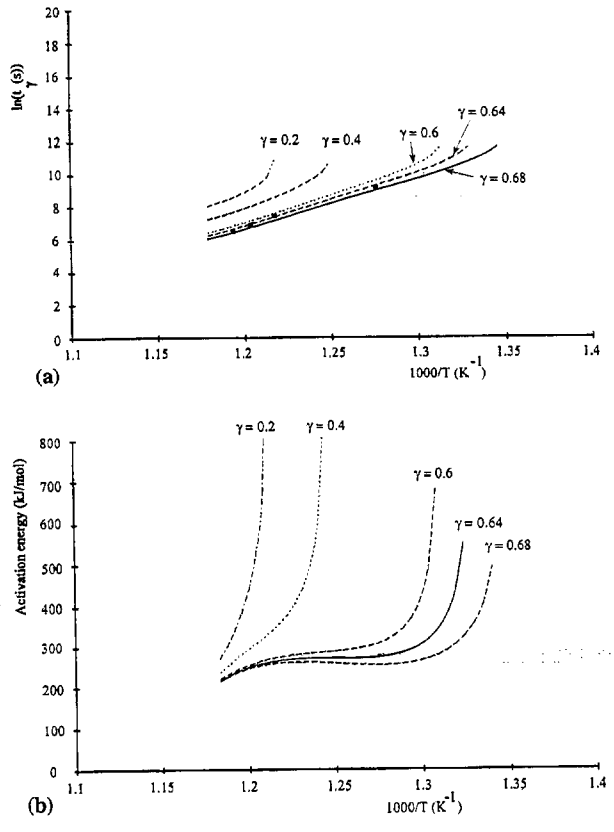

Fig. 9. The dissolution times for various iso-configurational states versus the reciprocal temperature taking into account the initial experimental particle size distribution. The squares indicate the annealing conditions used in the experiment yielding $\gamma = 0.64$ (a) and the apparent activation energies (b).

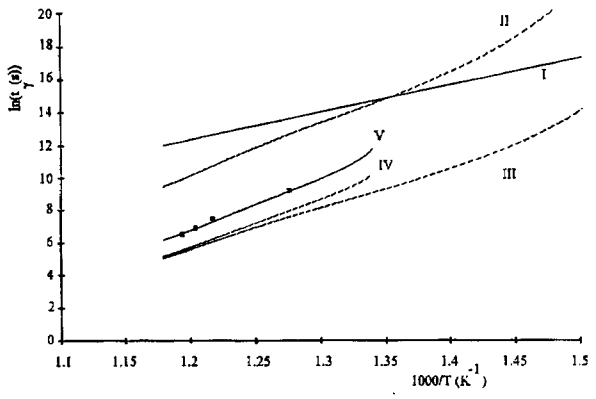

Fig. 10. Predicted dissolution times to obtain $\gamma = 0.64$ for various model assumptions (see text). All parameter values as determined on the experimental alloy. Squares indicate the conditions used in the experiment.

lution times are underestimated, as can be expected for the case of dissolution in an infinite medium. Curve IV applies to the situation of curve III but taking into account the finite cell size in which the particle dissolves. The soft impingement effects at the cell boundary lead to an increase in the annealing time required to reach the desired f_{res} value. It should be pointed out that in the transition from the conditions applying to curve III to those of curve IV the overall composition changes. In the case of curve III the average composition of the system approaches the initial matrix concentration (0.26 mass%), while in the condition of curve IV the average composition is taken to be equal to the true alloy composition, 1.35 mass%. The difference in average composition in the system explains why the dissolution times according to curve III become infinite at $T = 653$ K (the temperature at which the solid solubility is 0.28 mass%) while those according to curve IV do so at a temperature of 738 K (the temperature at which the solid solubility is 0.655 mass%). The dissolution times according to curve IV still underestimate the dissolution times required experimentally but the apparent activation energy is already predicted more or less correctly.

Finally, curve V describes the situation in which all factors, including those of the particle size distribution, are taken into account. At this degree of particle dissolution, $\alpha = 0.64$, the width of the particle size distribution leads to a deceleration of the dissolution process, in accordance with the results shown in Fig. 6, and a perfect agreement between experimental and predicted dissolution times is obtained. It is clear that all the factors mentioned above should be taken into account to predict the prevailing particle dissolution times and apparent activation energy correctly.

The theoretical results presented earlier indicate that the activation energy for dissolution of Si particles is by no means a constant but depends on a large number of parameters as well as the temperature range investigated. Such a variable activation energy for a diffusion phase transformation has also been observed and analysed in other studies, such as that of Berkenpas [15], who considered the case of simultaneous nucleation and growth, and that of Biglari et al [16], who considered the case of simultaneous precipitate formation and a phase transformation in the precipitate formed. In those studies the overlap or transition between two different processes, i.e. two rate limiting processes, was shown to be important in explaining the variations in activation energy. In contrast, the present case only deals with a single rate limiting process, the long range diffusion of silicon.

Okuda et al [17,18] used both the diffusion equation and Monte Carlo simulations to investigate the formation and dissolution of G.P. zones in binary Al–Zn-alloys. As the solubility of Al in Zn is not negligible, the concentration profile in the precipitate delayed the dissolution kinetics considerably during the early stages. This could contribute to the apparent activation energy as well. Since the solubility of Al in Si is negligible, this effect has not considered here.

Finally, although the model has been derived explicitly to describe the dissolution of Si particles in Aluminium, the model is applicable to any binary system with partial solubility for at least one of the components provided the temperature dependence of the mutual solubilities is known and the reaction proceeds under local equilibrium.

6. Conclusions

The dissolution kinetics of Si particles in an aluminium matrix can be described accurately by a model which takes into account long range diffusion of silicon, the temperature dependence of the solid solubility of silicon in aluminium, the shape of the particle, the finite cell size in which the particle can dissolve and the statistical distribution of the particle sizes. All factors have a significant effect on the dissolution kinetics and on the apparent activation energy for particle dissolution. The final apparent activation energy can deviate considerably from that for the diffusion of silicon in aluminium.

Acknowledgements

The authors acknowledge the stimulating remarks of Dr Ir.C. Vuik at the Applied Analysis Group at the faculty of Applied Mathematics and Informatics at the Delft University of Technology, 1996.

References

[1] M.J. Whelan, Met. Sci. J. 3 (1969) 95–97.
[2] U.L. Baty, R.A. Tanzilli, R.W. Heckel, Met. Trans. 1 (1970) 1651.
[3] U.H. Tundal, N. Ryum, Met. Trans. 23A (1992) 433.
[4] F.V. Nolfi Jr., P.G. Shewmon, J.S. Foster, Trans. Met. Soc. AIME 245 (1969) 1427.
[5] H.B. Aaron, G.R. Kotler, Met. Trans. 2 (1971) 393.
[6] F.J. Vermolen, S. Van der Zwaag, Mater. Sci. Eng. A220 (1996) 140–146.
[7] H.M. Slabbekoorn, Msc. thesis, Delft University of Technology, 1996.
[8] D.W. Trim, Applied Partial Differential Equations, P.W.S. Kent, Boston, 1990.
[9] J. Crank, Free and Moving Boundary Problems, Clarendon Press, Oxford, 1984, p. 1.
[10] C. Vuik, The Solution of a One-dimensional Stefan Problem, Centrum voor Wiskunde en Informatica, Amsterdam, 1993.
[11] S. Fujikawa, K. Hirano, Y. Fujikawa, Met. Trans. A. 9A (1978) 1811.
[12] L.F. Mondolfo, Aluminium Alloys, Structure and Properties, Butterworth, London, 1976, pp. 253–278, 368–376.
[13] S.V. Patankar, Numerical Heat Transfer and Fluid Flow, Hemisphere Press, Washington, 1980.
[14] Underwood, Quantitative Stereology, Addison-Wesley, Reading, 1970.
[15] M.B. Berkenpas, J.A. Barnard, R.V. Ramanujan, H.I. Aaronson, Scr. Met. 20 (1985) 323.
[16] M.H. Biglari, C.M. Brakman, E.J. Mittemeijer, S. Van der Zwaag, Philos. Mag. A 72 (1995) 931.
[17] H. Okuda, K. Osamura, Trans. ISIJ 28 (1988) 809–817.
[18] H. Okuda, K. Osamura, Y. Amemiya, H. Hashizume, Mater. Trans. JIM 30 (11) (1989) 886–894.